RESEARCH PAPER

Multi-scale finite element simulation on large deformation behavior of wood under axial and transverse compression conditions

Weizhou Zhong[1,2] · Zexiong Zhang[1,2,3] · Xiaowei Chen[4,5] · Qiang Wei[1,5] · Gang Chen[1] · Xicheng Huang[1]

Abstract

Multi-scale finite element method is adopted to simulate wood compression behavior under axial and transverse loading. Representative volume elements (RVE) of wood microfibril and cell are proposed to analyze orthotropic mechanical behavior. Lignin, hemicellulose and crystalline-amorphous cellulose core of spruce are concerned in spruce nanoscale model. The equivalent elastic modulus and yield strength of the microfibril are gained by the RVE simulation. The anisotropism of the crystalline-amorphous cellulose core brings the microfibril buckling deformation during compression loading. The failure mechanism of the cell-wall under axial compression is related to the distribution of amorphous cellulose and crystalline cellulose. According to the spruce cell observation by scanning electron microscope, numerical model of spruce cell is established using simplified circular hole and regular hexagon arrangement respectively. Axial and transverse compression loadings are taken into account in the numerical simulations. It indicates that the compression stress–strain curves of the numerical simulation are consistent with the experimental results. The wood microstructure arrangement has an important effect on the stress plateau during compression process. Cell-wall buckling in axial compression induces the stress value drops rapidly. The wide stress plateau duration means wood is with large energy dissipation under a low stress level. The numerical results show that loading velocity affects greatly wood microstructure failure modes in axial loading. For low velocity axial compression, shear sliding is the main failure mode. For high velocity axial compression, wood occur fold and collapse. In transverse compression, wood deformation is gradual and uniform, which brings stable stress plateau.

Keywords Multi-scale model · Representative volume element · Spruce · Energy dissipation · Wood cell

1 Introduction

As a low density and natural material, wood is conveniently available and used widely in civil building, product packaging and papermaking fields. Wood microstructure is made up of regular array polymeric constituent cells, which consists of much microfibril with different distribution angle. The cell array pattern leads to wood anisotropic mechanical properties [1, 2]. Three symmetry axes of axial, radial and tangential can be defined according to wood cell array pattern. Wood mechanical properties in radial and tangential orientations are almost similar, so transverse isotropy constitutive model is usually applied to describe the mechanical behavior. Taking wood anisotropy behavior and microstructure distribution into account, many studies on wood macro mechanical behavior and cell array pattern were performed in recent years [3–5]. Wood mechanical properties in different loading orientations can be obtained using conventional material testing experiments. For example, material testing

✉ Weizhou Zhong
zhongwz@caep.cn

1   Institute of Systems Engineering, China Academy of Engineering Physics, Mianyang 621999, Sichuan, China

2   Shock and Vibration of Engineering Materials and Structures Key Laboratory of Sichuan Province, Mianyang 621999, Sichuan, China

3   College of Engineering Science, University of Science and Technology of China, Hefei 230026, Anhui, China

4   Advanced Research Institute for Multidisciplinary Science, Beijing Institute of Technology, Beijing 100081, China

5   The State Key Lab of Explosion Science and Technology, Beijing Institute of Technology, Beijing 100081, China

machine INSTRON is used to test wood quasi-static and low strain rate mechanical property. Hopkinson bar equipment is applied for high strain rate mechanical property [6, 7]. Scanning electron microscope is applied to observe the cell size and array [8–10].

Wide plastic stress plateau is a typical characteristic for wood compression stress–strain curve, which is similar to foam material. In compression process, wood cell wall buckling goes into the cell lumens. Once the lumens available for cell wall buckling become limited, compression stress increases significantly with strain [11–13]. Owing to the wide stress plateau, wood is taken as a cushion material for high velocity impact events, and is widely used as an impact energy absorbing material at the design of the transportation flasks for nuclear fuel [14, 15]. It exits many literatures on wood elastic–plastic and facture properties. For wood quasi-static and dynamic mechanical properties, Brüchert [16] pointed out that the flexural stiffness of trees is mainly influenced by stem radius, resulting in a higher flexural stiffness for thicker trees. Widehammar [17], Buchar [18] and Holmgren [19] investigated the influence of strain rate, moisture content and loading direction on the stress–strain relationships for oak, beech, pine, spruce and birch wood. It shows that the wood properties are sensitive to the loading conditions. Vural [20] and Uhmeier [21] developed an encapsulated SHPB device for wood testing, and investigated wood dynamic compression behavior at high deformation rate, temperature, and pressure conditions. Some literatures [22–24] also show Hopkinson equipment is widely applied to investigate wood strain rate sensitivity.

Wood cell structure affects greatly its macro-mechanical properties. Advanced electronic instrument are applied to observe fiber and cell wall deformation behavior in the literatures. Keckes [25] combined tensile tests on individual wood cells and on wood foils with simultaneous synchrotron X-ray diffraction analysis. It indicates that tensile deformation beyond the yield point does not deteriorate the stiffness of either individual cells or foils. Clair [26] observed wood longitudinal shrinkage is much more important in gelatinous layer than in other layers by scanning electron microscope. Salmén [27] discussed the relations between elastic properties of fiber, the matrix structure and the wood polymer elastic constants. It shows longitudinal elastic modulus of cellulose dominates the longitudinal fiber properties and amorphous polymers play a more important role in the transverse direction. Some literatures [28, 29] are focused on wood fiber and cell property, which show how wood microstructure dominates macro deformation and main failure modes.

With computation technique developing, numerical simulation becomes an economical and effective way in investigation on wood mechanical property. Vasic [30, 31] introduced some numerical models for wood fracture and explored avenues toward achieving models for wood fracture that are both appropriate and robust. Dubois [32] used a generalized Kelvin–Voigt model to analyzed linear viscoelastic behavior and strain accumulation during moisture content changes in wood. Saavedra Flores [33, 34] provided a coupled multi-scale finite element model for the constitutive description structure of wood cells. Representative volume element (RVE) is proposed to represent wood cell array. Clouston [35] formulated a nonlinear stochastic model to simulate the stress–strain behavior of strand-based wood composites based on the constitutive properties of the wood strands. The nonlinear constitutive behavior of the wood strands is characterized within the framework of rate-independent theory of orthotropic plasticity. It can be seen that numerical analysis is beneficial supplement of wood experiment investigation. Numerical simulation can provide not only the detailed material deformation process, but also the mechanical parameter changing during loading process [36, 37].

In the previous literatures, many studies have focused on wood property under different velocity loading, ambient temperature and moisture content conditions. Strain rate, temperature and density effects on wood property were described by experiment and numerical simulations. But the relationship between wood macro-mechanical property and micro-structure array is little discussed. Wood micro-structure array leads to the anisotropic characters. As the dimension scale changes from nanometer to micrometer level between wood microfibril and cellular cell, it is necessary to analyze wood tissue structure influence on the mechanical behavior by multi-scale numerical models. In the present work, representative volume elements of microfibril and cellular cell are proposed to discuss wood anisotropic mechanical property. Nanoscale model simulation of spruce microfibril, including lignin, hemicellulose and crystalline-amorphous cellulose core, is performed to analyze the equivalent mechanical parameters. Spruce cell microstructure with circular holes and regular hexagon array are established under axial and transverse compression conditions respectively. The stress plateau and main failure modes are obtained by numerical simulations under different loading conditions. Based on the simulation results, loading orientation and velocity influence on wood microstructure failure mode is discussed.

## 2 Mechanical behavior of spruce in three symmetry axes

2.1 Macro-mechanical behavior of spruce

Tree is a natural composite of high tension strength cellulose fibers embedded in a matrix of lignin. Its growing speed varies in different temperature, humidity and sunlight

conditions. Growing speed difference in a year induces annual rings on cross section. Microstructure array pattern defines mainly spatial symmetry distribution of wood mechanical property. For a wood specimen cutting from tree, three symmetry axes of axial, radial and tangential can be assigned. Axial is consistent with tree growth orientation. Radial is orthogonal to annual ring and tangential is tangent to annual ring in long grained section, shown in Fig. 1.

In the present work, cylinder wood specimens are cut from a spruce, which diameter is 610 mm, moisture content is 12.72% and the density is 413 kg/m^3. As some defect occurs in the tree center, specimen is usually cut away from heartwood. The diameter of cylinder specimen is 40 mm and the height is 30 mm. The specimen section size is over 100 times than spruce cell pore. It ensures the experimental result reflects the wood macro-mechanical behavior. Wood specimen axis is consistent with the intended material orientation. The cutting scheme is shown in Fig. 1. The cylinder axis is in tree growth direction for axial compression specimen. Axes of radial, tangential compression specimens are orthogonal, tangent to the annual rings in long grained section respectively.

Spruce quasi-static compression tests are implemented by conventional material experiment machine. The loading velocity is 0.01 mm/s and the stress–strain curves in the three material axes are shown in Fig. 2. It indicates that wood goes through elastic, yield and compaction phases during a large compression deformation process. It shows the stress strength in axial orientation is much larger than that of radial and tangential orientations. For axial compression, stress plateau decreases with strain increasing and appears 'plastic softening' phenomenon. The axial compression elastic modulus is 11,330 MPa and the yield stress is 37.8 MPa.
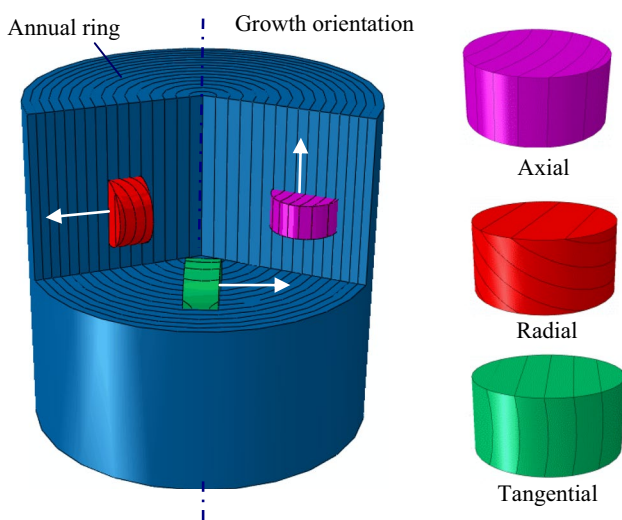
Fig. 1 Cutting scheme of wood specimen in axial, radial and tangential orientations
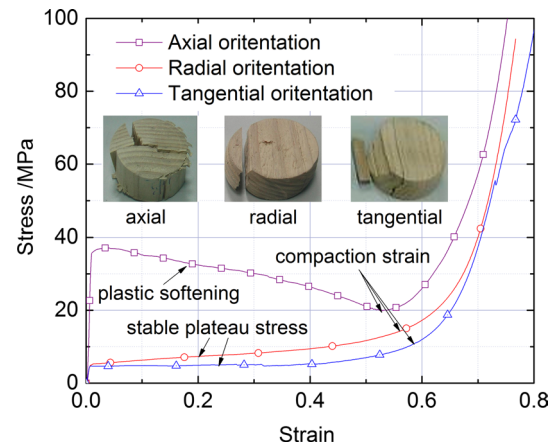

Fig. 2 Compression stress–strain curves of different loading orientations in experiments

For radial and tangential compression, deformation process is relatively stable, and stress increases with strain. The radial elastic modulus is 532 MPa and the yield stress is 4.42 MPa. The tangential compression elastic modulus is 351 MPa and the yield stress is 4.40 MPa. The compaction strains of axial, results of radial and tangential compression are similar and stress increases greatly with strain when plastic deformation is over 0.6.

The typical compression failure modes along different orientations are shown in Fig. 2. It indicates that the axial compression failure behavior is different from the radial and tangential compression. In the axial loading, compression force induces wood circumferential tension failure. When the loading orientation is consistent with radial or tangential orientation, the main failure modes are wood fiber slippage and delamination. Being different from axial compression, the radial and tangential compression deformation is a steady-state process. Wood cell is collapsed gradually in compression process. The stable failure behavior induces a wide stress plateau region in radial and tangential compression conditions.

2.2 Microstructure deformation feature of spruce

Spruce is a coniferous evergreen tree species, which is a heterogeneous, hygroscopic, cellular and anisotropic material. Cell wall is composed of micro-fibrils of cellulose and hemicellulose impregnated with lignin [38]. Cell microstructure of spruce is shown in Fig. 3 by scanning electron microscope. It shows that there are many small circle pits in the cell walls, and the tracheids are uniform. Pits in the cell wall are typical feature for coniferous tree. Tracheids diameter is usually from 20 μm to 80 μm.
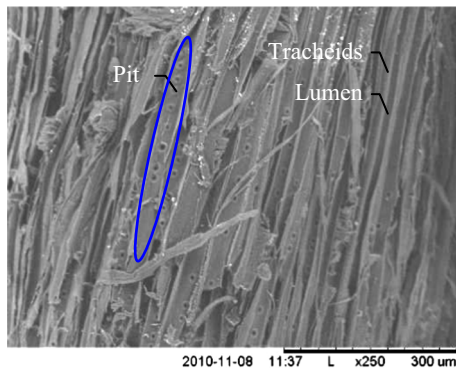
Fig. 3 Spruce microstructure without deformation in radial section
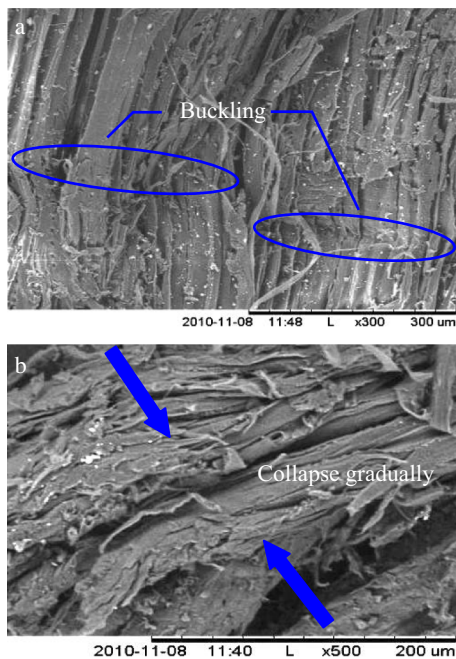
Fig. 4 Typical deformation of axial compression in radial section (**a**) and transverse compression in tangential section (**b**)

Microstructure deformation of axial compression is shown in Fig. 4a. Buckling appears in the middle of cell wall. The thin cell wall structure is liable to compressive instability. Cell wall buckling brings an abrupt decreasing point in axial compression stress–strain curve in Fig. 2. The macroscopical deformation reflects compression folds on the surface of wood specimen [22]. For radial and tangential transverse compression, the microstructure deformations are similar. The typical deformation mode is shown in Fig. 4b. It shows wood cell collapse process is gradual and stable during the whole compression process, which induces wide stress plateau region in radial and tangential compression in Fig. 2.

3 Nanoscale numerical model of spruce microfibril

3.1 Structure feature of spruce microfibril

For spruce cell wall structure, three major chemical constituents of cellulose, hemicellulose and lignin are contained, shown in Fig. 5. Cellulose mass fraction varies from 40 to 50% in the weight of wood substance. Hemicellulose is 15–25% and lignin is 15–30% respectively [39]. Cellulose is a long glucose polymer unit which is organized into periodic crystalline and amorphous regions along the core. The periodic array is covered by amorphous cellulose outer layer. Crystalline mass fraction affects cellulose stiffness and amorphous provides cellulose flexibility [40]. Hemicellulose is a polymer with little strength. Its mechanical property is greatly sensitive to moisture. High water content induces hemicellulose strength softening. Lignin is related with wood cell shear strength. It is a kind of amorphous polymer, which cement many individual cells together. As lignin is a hydrophobic component, its mechanical property is relatively stable with different moisture contents. Though the main constituents of cellulose, hemicellulose and lignin, compose a complicated mechanical character, the spatial arrangement of microfibrils can be considered as a periodic block of rectangular cross-section with infinite length.

Detailed dimensions of wood microfibril finite element model are shown in Fig. 5. It is difficult to define the bond states of the different constituents of wood microfibril. Sharing nodes of different constituents are chosen in the following simulation. It is reliable way for compression case if the model stiffness increasing is ignored. But sharing nodes will induce great error for wood tension numerical simulation. The parameters are referred from the literatures [41–43]. The side length of microfibril cross section is 6.6 nm. Donaldson [41] measured the thickness of cellulose using transmission electron microscopy and provided the average value 3.6 nm. Amorphous cellulose core and amorphous sheeting are parts of the cellulose. Amorphous sheeting surrounds amorphous cellulose core and crystalline cellulose. Andersson [42] determined the thickness of amorphous cellulose core and crystalline is 3.2 nm. The thickness of amorphous sheeting is taken as 0.2 nm. The mean length of 36.4 nm is taken for crystalline fraction and 18.9 nm is for amorphous cellulose in crystalline and amorphous periodic array. Hemicellulose covers the cellulose surface and its thickness is 0.8 nm. Lignin locates in the outer layer and the thickness is 0.7 nm [43].

3.2 Mechanical properties of wood constituents

The basic mechanical properties of wood constituents are shown in Table 1. For mechanical behavior of lignin,
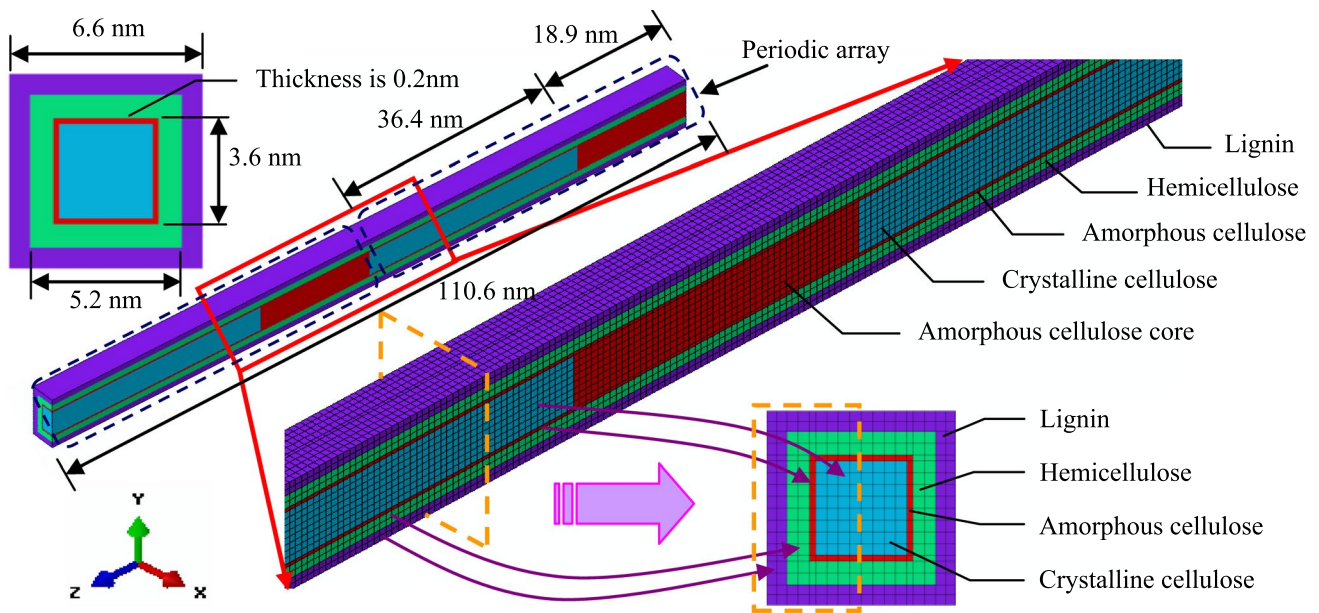
Fig. 5 Schematic of typical wood microfibril with periodic rectangular cross-section unit array

hemicelluloses and amorphous, the plastic hardening modulus is little and isotropic elastic-perfectly plastic constitutive model is adopted. Density of the lignin is 1450 kg/m^3. Young's modulus is 1.56 GPa and Poisson's ratio is 0.3 [27]. Hemicellulose and amorphous is with same density of 1500 kg/m^3. Young's moduli of hemicellulose and amorphous are 0.04 GPa and 10.42 GPa respectively. Poisson's ratios of 0.2 and 0.23 are taken for hemicellulose and amorphous respectively [34, 44]. The yield strengths of lignin, hemicelluloses and amorphous are taken as 19 MPa, 20 MPa and 800 MPa respectively. Crystalline is taken as perfectly elastic material and anisotropic constitutive model adopted for the numerical simulation. Density of crystalline is taken as 1590 kg/m^3. Crystalline anisotropic elastic constants are shown in Table 1 [45]. The highest strength orientation is consistent with microfibril axis. The anisotropic constitutive model of crystalline is transverse isotropy in cross section. Mechanical properties of the other two orientations are identical. Material constituent behavior and microstructure array will bring varied mechanical response in different loading velocity conditions. In the following impact simulations, wood constituent is simplified as rate independent and microstructure array is taken into account to investigate on influence of loading velocity for spruce microstructure deformation.

According to the wood microfibril model dimension in Fig. 5 and the constituent densities in Table 1, the volume fraction and mass fraction of constituent material are calculated, shown in Table 2. It indicates that lignin is with the highest volume and mass fractions, which are 37.93% and 36.79% respectively. Hemicellulose is with the second highest volume and mass fractions of 32.32%, 32.43%. The volume and mass fractions of crystalline are 15.47% and 16.45%. For amorphous content, the volume and mass fractions are 14.28% and 14.33% respectively.

3.3 Numerical simulation on mechanical behavior of microfibril

Finite element software ABAQUS/Explicit is applied to simulate spruce microfibril compression behavior. The nanoscale model of microfibril is shown in Fig. 5. The numerical model is meshed by C3D8R element, including 99,997 nodes and 89,424 elements. Compression load is applied on specimen end section and along the microfibril axis. The other end of specimen is fixed in the simulation. Microfibril compression response under quasi-static axial loading is simulated. The Mises stress and equivalent plastic strain distribution of microfibril are shown in Fig. 6. Taking wood microfibril constituent diversity into account, the half microfibril model is displayed to observe the inner mechanical property information easily. It shows the high stress region converges on the inner crystalline and amorphous celluloses in Fig. 6a. As the two constituents are with relatively higher moduli, it induces higher stress value in the interior of microfibril. Heterogeneity of wood microfibril constituent distribution and the properties bring a large deformation occurring in the weaker region, shown in Fig. 6b. Amorphous cellulose is taken as hyperelastic material in the simulation. Buckling phenomenon appears between the two amorphous celluloses in axial compression

Table 1 Mechanical properties of lignin, hemicellulose, amorphous and crystalline [27, 34, 44, 45]

Constituent	Density (kg m^{-3})	Young's Modulus (GPa)			Poisson's Ratio		
Lignin	1450	1.56			0.30		
Hemicellulose	1500	0.04			0.20		
Amorphous	1500	10.42			0.23		
		E_{11}	E_{22}	E_{33}	ν_{12}	ν_{23}	ν_{31}
Crystalline	1590	134.00	27.20	27.20	0.05	0.50	0.05

Table 2 Volume and mass fractions of constituents in wood microfibril

Classification	Lignin	Hemicellulose	Amorphous	Crystalline
Volume fraction (%)	37.93	32.32	14.28	15.47
Mass fraction (%)	36.79	32.43	14.33	16.45

process. It indicates wood microfibril deformation is non-uniform even if quasi-static compression condition.

Figure 7 presents compression stress–strain curve of microfibril in axial loading. It shows that microfibril buckling induces the stress decreasing abruptly under a small strain condition. The buckling deformation induces the stress value decreasing greatly. Owing to buckling process, the curve characteristic reflects the microfibril microstructure response, much more than the material mechanical behavior.

According to the initial linear phase of the stress–strain curve, the equivalent elastic modulus of microfibril E_{eq} can be obtained from

$$E_{eq} = \frac{d\sigma}{d\varepsilon}, \tag{1}$$

where σ and ε are stress and strain respectively. The equivalent density ρ_{eq} can be obtained from

$$\rho_{eq} = \sum_{i=1}^{n} \rho_i V_i, \tag{2}$$

where V_i and ρ_i are spruce constituent volume fraction and density respectively. The equivalent mechanical properties of spruce microfibril are shown in Table 3. The microfibril equivalent elastic modulus is 5.84 GPa. Equivalent density is 1490 kg/m^3 and Poisson's ratio is taken as 0.4 approximately. With the equivalent spruce tissue property parameters, a simplified numerical simulation on microscale spruce cell model can be performed in the following present work.

4 Microscale numerical model of wood cell

The Fig. 3 shows spruce cell is porous structure with many pits in the wall. Vural [20] observed wood cell shape and dimension by scanning electron microscope. Most pore sections are like regular hexagon and the other pores look like circle. The section size of cell microstructure varies from 15 to 60 μm. The cell arrangement leads to wood macroscopic mechanical behavior anisotropy. So a representative volume element (RVE) can be adopted to simplified analyze wood compression anisotropic behavior and failure mechanism. The RVE contains over 10 cell pores along different direction to convince the model
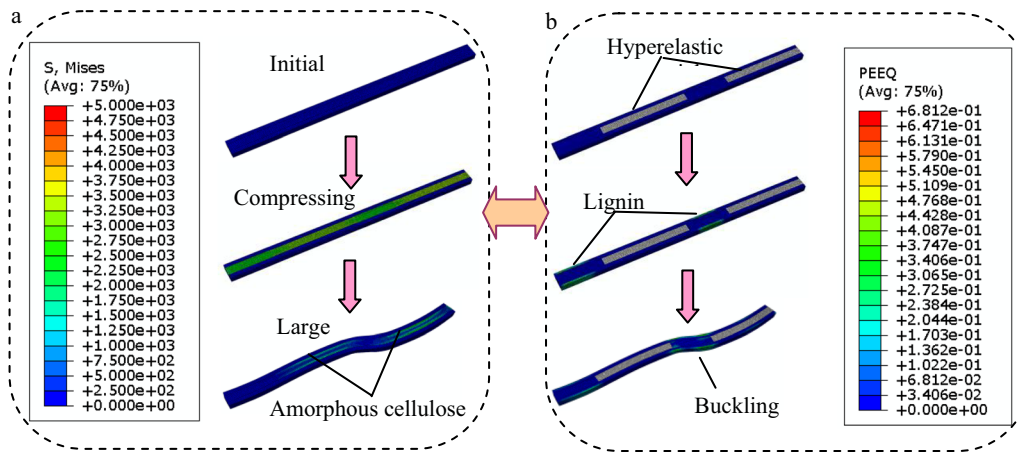
Fig. 6 Mises stress (**a**, unit:MPa) and plastic strain (**b**) distribution of wood microfibril during compression process
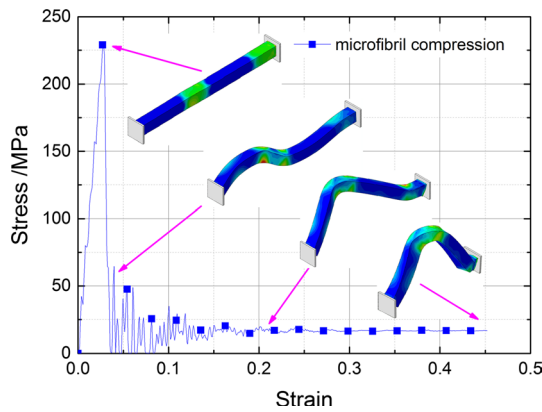

Fig. 7 Compression stress–strain curve of wood microfibril

Table 3 Equivalent mechanical properties of spruce microstructure tissue

Name	Density (kg/m³)	Young's modulous (GPa)	Poisson's ratio
Spruce tissue	1490	5.84	0.4

creditability [46]. Two kinds of RVE models with hexagon and circle pores, which are subjected to axial and transverse loading, are discussed respectively in the following simulations.

4.1 Microstructure of spruce cell with hexagon pores

The detailed dimension of wood microstructure model with hexagon pores is shown in Fig. 8. Considering numerical analysis validity and efficiency, the pits in spruce cell walls are ignored in the simplified simulation model. The RVE model is a cube and the side length is 425 μm. Cell wall thickness is 5 μm. Porosity of hexagon pore microstructure model is 73.27%. There are 417,298 nodes and 287,680 hexahedral elements in the RVE model. The whole model is meshed using C3D8R reduced integration element and general contact is chosen in ABAQUS explicit procedure. The loading is applied on the RVE model upper surface and the bottom is constraint along the loading direction in the simulation. The equivalent mechanical property parameters in the Table 3 are used for RVE simulation.
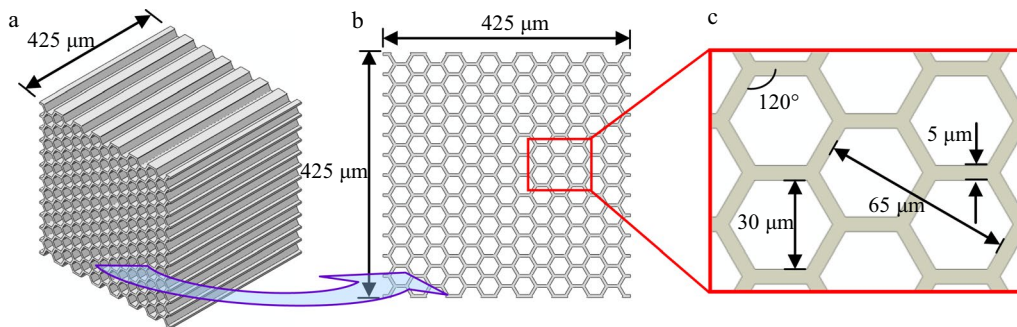

Fig. 8 Wood microstructure model with regular hexagon pores. **a** 3-D model, **b** surface with pores, **c** detailed view of surface

4.2 Microstructure of spruce cell with circular pores

The RVE model of spruce microstructure with circular pores is shown in Fig. 9. The model is also a cube and the side length is 420 μm. The radius of circular pore is 15 μm. Distance between centers of two adjacent pores is 35 μm, which is equivalent to that of RVE model with hexagon pores. But the cell wall thickness is not constant. The thickness of the thinnest position is 5 μm. Porosity is 66.28% for the RVE model. The numerical model contains over 228,480 nodes and 164,920 hexahedral elements. In contrast to the previous model in Fig. 8, C3D8R reduced integration element is adopted in the model meshing. The mechanical property parameters in the Table 3 are applied to describe the RVE material properties in the simulation.

5 Large deformation behavior of wood under axial compression

5.1 Large deformation of wood RVE with hexagon pores under axial compression condition

Quasi-static axial compression behavior of spruce RVE with hexagon pores is simulated. The compression stress-stain curve is shown in Fig. 10. The curve presents three deformation phases of spruce microstructure in axial compression process. The RVE goes through a short linear elastic deformation. An inclined shear band occurs in the microstructure model. The angle between axial loading direction and shear band is about 45°. Stress decreases greatly with loading displacement increasing when the strain is from 0.1 to 0.2. Then the stress goes into a long stable plateau phase. It indicates that the gradual shear sliding leads to a wide plateau stress in the stress–strain curve. The compact
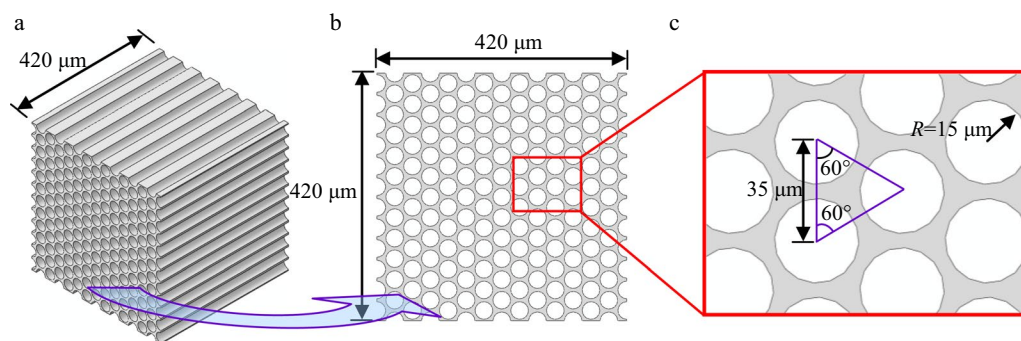

Fig. 9 Dimension of wood microstructure model with circle pores. **a** 3-D model, **b** surface with pores, **c** detailed view of surface
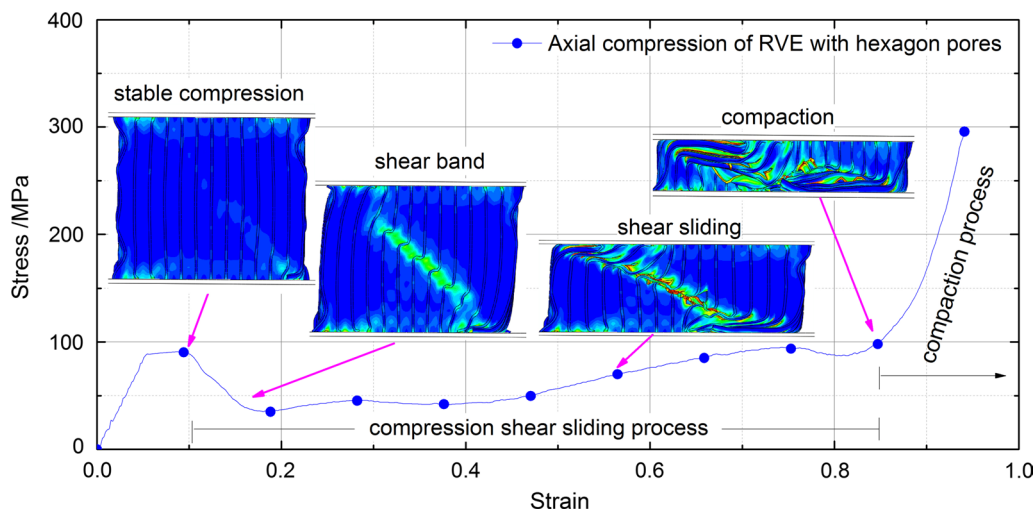

Fig. 10 Axial compression stress–strain curve of RVE with hexagon pores

phase occurs when the strain reaches about 0.85 and stress increases quickly with strain in the curve.

Detailed deformation process of RVE model in axial compression is shown in Fig. 11. Shear sliding in 45° direction and collapse are the main failure modes for wood microstructure in axial compression. Buckling and wrinkle occur on the side wall during compression process. It means that the main energy dissipation modes are cell wall shear sliding and collapse for wood axial compression. Collapse and buckling occur at the strain 0.1, which induces the compression stress decreases quickly in the Fig. 10.

5.2 Large deformation of wood RVE with circular pores under axial compression condition

Taking the distance between centers of two adjacent pores as a constant 35 μm, RVE model with circular pores subjected to quasi-static axial compression loading is simulated. Figure 12 shows the stress–strain curve of the RVE model in the axial loading. The curve shape is similar to that of the hexagon RVE model in Fig. 10. Three phases of elastic deformation, yield plateau and compression compaction are distinct in the curve. Due to difference of pore shape and porosity, the first stress plateau is higher than that of the hexagon model. When the strain reaches about 0.18, stress decreases abruptly in Fig. 12. The strain is larger than that of the RVE with hexagon pores. Stress goes through a stable phase when the strain is from 0.25 to 0.85. Stress increases greatly with strain when the strain is over 0.85. Being similar to the hexagon RVE, 45° shear band occurs in the circular pore model. Gradual shear sliding is related to the wide stable stress plateau in stress–strain curve.

The RVE model deformation processes at several strain conditions are shown in Fig. 13. The failure modes are
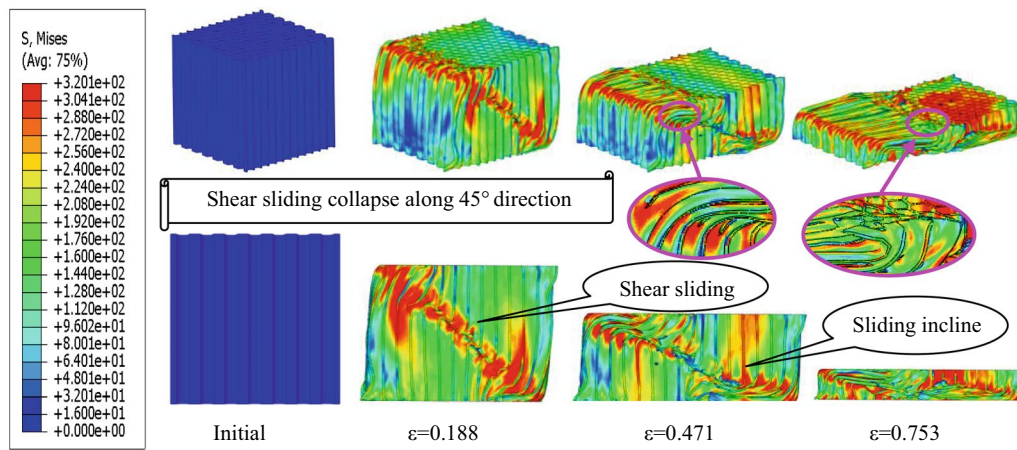

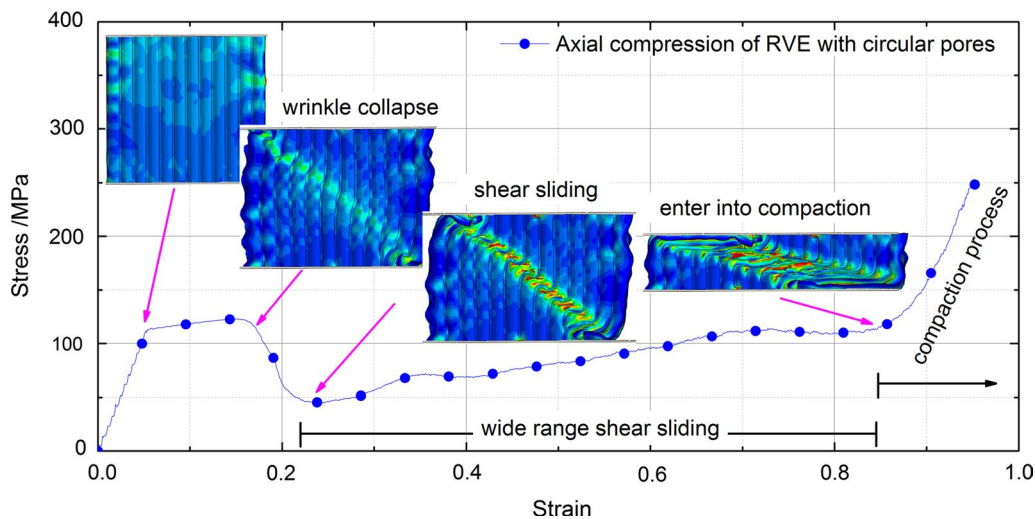**Fig. 11** Axial compression collapse process of RVE with hexagon pores (unit: MPa)

Fig. 12 Axial compression stress–strain curve of RVE with circular pores
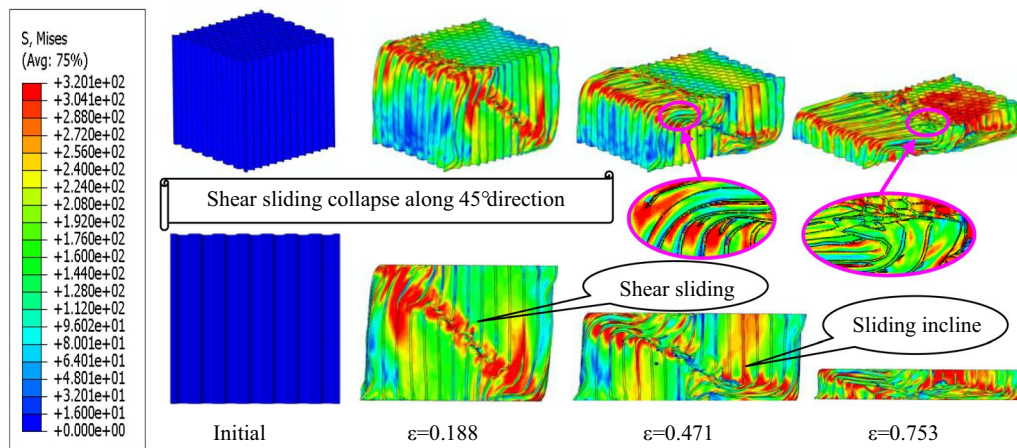
Fig. 13 Axial compression collapse process of RVE with circular pores (unit: MPa)
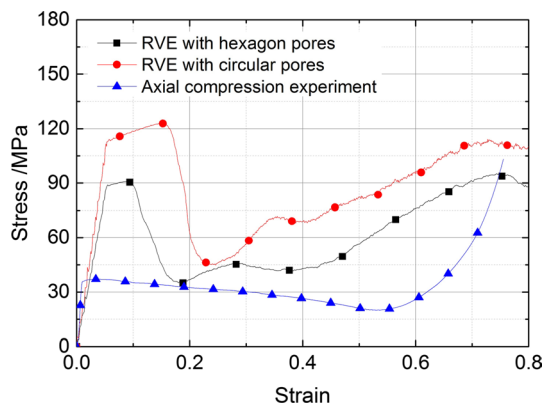

Fig. 14 Axial compression curve comparison for different approaches

similar to the hexagon model in Fig. 11. Shear sliding along 45° direction and collapse are the main modes in axial compression. The side surfaces are compressed fold, which is moving from the top to the bottom in Fig. 13. The shear band becomes into two bands when compression strain reaches 0.5. The band orientations are also along 45° direction, which brings much more energy dissipation during compression process.

5.3 Comparison of different pore shape response in axial compression

Stress–strain curve comparison between the different RVE models and the experimental result is shown in Fig. 14. It shows numerical simulation curves are larger than the experimental result. The stress decreasing is much sharper for the simulation result. The reason is that the pits and water in cell structure are ignored in the RVE model. Pits usually weaken structure strength and water contributes to yield buckling deformation. The RVE model with ideal cell microstructure

distribution induces the higher yield stress and plateau level. For wood axial compression, the ignoring factors lead to the difference between the simulations and the experimental results.

Though the two RVE models are with the minimum cell wall thickness 5 μm, pore shape diversity brings porosity difference. Porosity 73.27% of RVE with hexagon pores is larger than 66.28% of RVE with circular pores. The lower porosity results in a higher and wider elastic–plastic plateau, and the elastic limit strain difference is about 0.06 in Fig. 14. Plastic plateau stress of the circular model is 22 MPa higher than that of the hexagon model. The results show that pore shape and distribution pattern is also one of the main influence factors in wood RVE numerical simulation. According to the experimental results, the RVE model of hexagon pores is with better simulation results than that of the RVE model with circular pores.

6 Large deformation behavior of wood under transverse compression

6.1 Large deformation of wood RVE with hexagon pores under transverse compression condition

Mechanical response of spruce RVE with hexagon pores under quasi-static transverse compression is simulated. The compression stress–strain curve is shown in Fig. 15. It shows that the stress increases monotonously with strain. Three deformation phases of elastic deformation, plastic plateau and compaction appear in the curve. Hexagon pores are compacted gradually during compression process. The stress plateau is stable when strain is from 0.09 to 0.68. Comparing with the axial compression, the plateau stress is much smaller. Lateral expansion deformation of spruce microstructure is tiny in compression process.
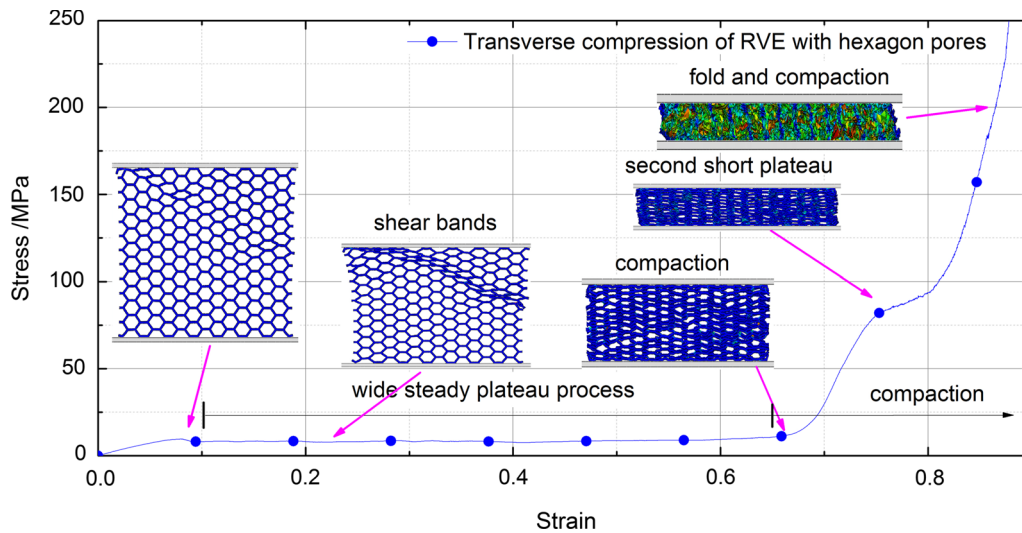
Fig. 15 Transverse compression stress–strain curve of RVE with hexagon pores

It can be taken as volume compressible behavior. When the strain reaches about 0.75, the second plateau occurs and lateral expansion becomes obvious. The subsequent compaction brings the stress increases greatly in Fig. 15.

The detailed deformation process under transverse compression is shown in Fig. 16. It indicates the RVE cube microstructure cell is compressed into a flat plate. The whole process is stable and uniform. The wall is gradually folded, which is like foam material compression phenomenon. Some shear bands appear on the pore surface during compression process. The angle between shear bands and loading orientation is about 45°. It indicates that the main energy dissipation modes are cell wall folding and collapse for wood transverse compression.

6.2 Large deformation of wood RVE with circular pores under transverse compression condition

Figure 17 shows the stress–strain curve of RVE with circular pores under transverse compression. The curve is similar to that of the hexagon pore model in Fig. 15. It increases monotonously with strain, including elastic deformation, plastic plateau and compaction. Being different from RVE with hexagon pores, stress oscillation appears at the beginning of plastic deformation in the circular model. The circle collapsing on the both ends leads to stress oscillation. There are two small troughs of the stress oscillation, which is related to the both ends' cell collapse respectively. The plastic plateau stress is stable when strain is from 0.1 to 0.6. When the strain is lower
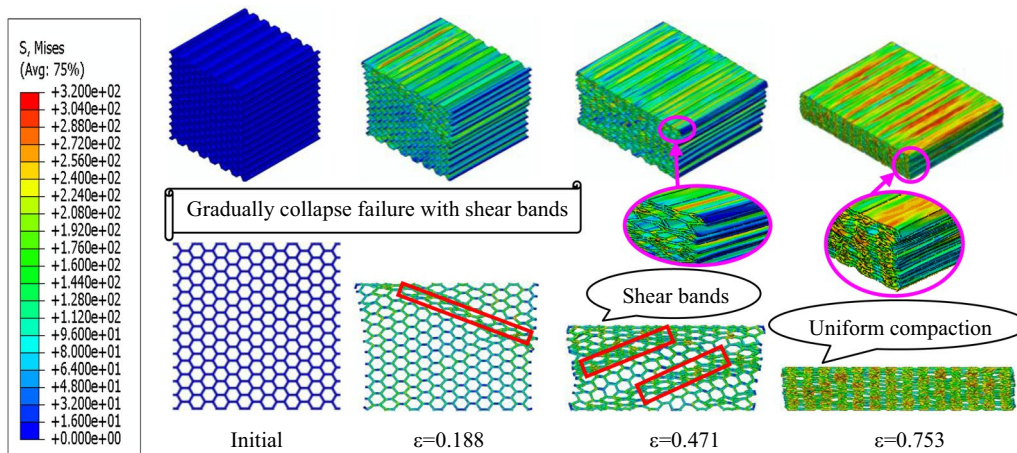

Fig. 16 Transverse compression collapse process of RVE with hexagon pores (unit: MPa)
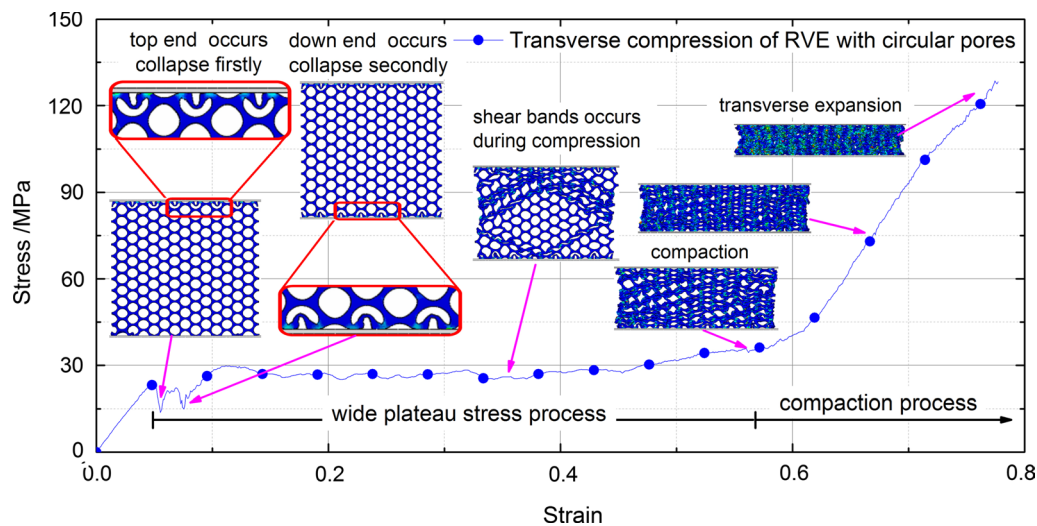
Fig. 17 Transverse compression stress–strain curve of RVE with circular pores

than 0.6, lateral deformation is very tiny. When the strain increases in compaction phase, the lateral deformation increases greatly and finally becomse flat.

Detailed deformation process of RVE model with circular pores under transverse compression is shown in Fig. 18. Being similar to hexagon pore model, 45° shear collapse and folds are the main failure modes in transverse compression. Some shear bands appear during the compression process, and folds occur on the side surfaces marked by ellipse. The stale compression plastic deformation induces the wide plateau stress. Being same as hexagon pore model, the main energy dissipation modes are cell wall folding and collapse in transverse compression.

6.3 Comparison of different pore shape response in transverse compression

The stress–strain curves of numerical simulations and experiments in transverse compression are shown Fig. 19. It indicates that the result of hexagon pore RVE curve is consistent with the experimental results. On the contrary, the result of circular pore model is with higher stress level. The porosity and pore shape of RVE model with circular pore induce the phenomenon. According to the simulation results, Hexagon pore model is superior to circular pore model. In contrast to axial loading, the radial and tangential compression deformation process is much more stable. Stress increases monotonously in transverse compression. The deformation is uniform distribution in the model structure. Comparing to axial simulation results, the numerical simulation curves of
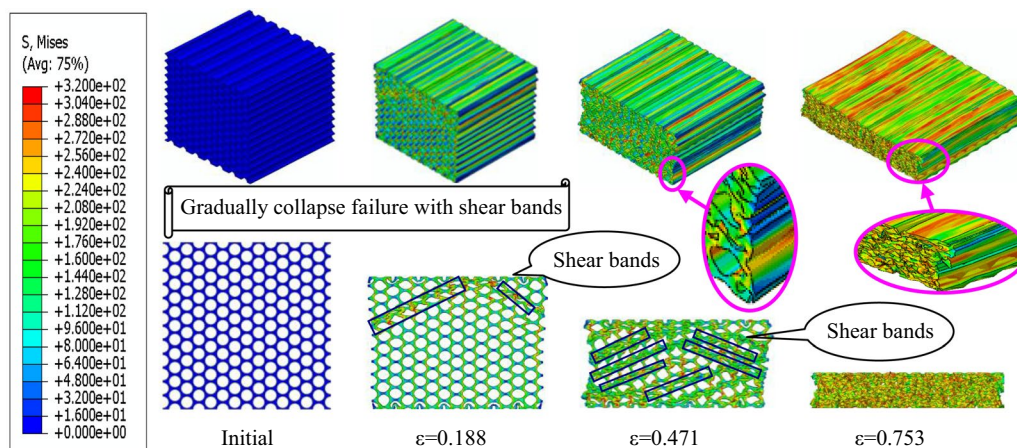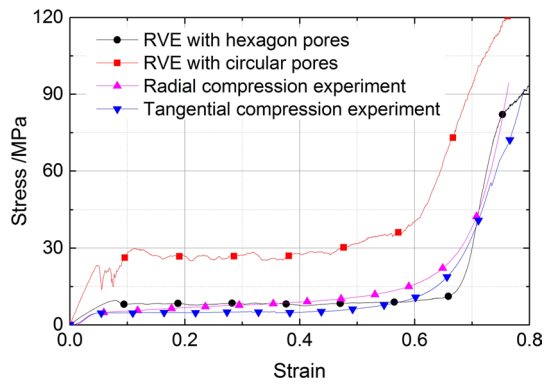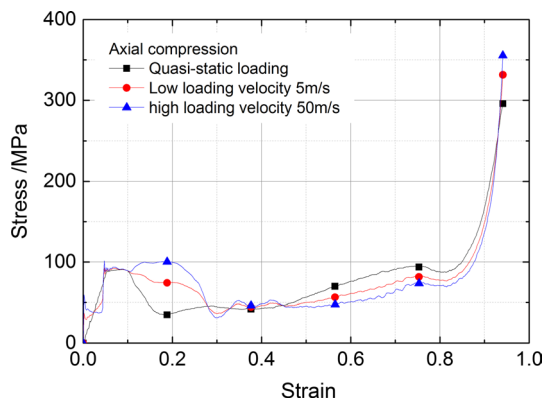

Fig. 18 Transverse compression collapse process of RVE with circular pores (unit: MPa)

Fig. 19 Transverse compression curve comparison of different approaches

Fig. 20 Stress-strain curve comparison of different loading velocities under axial compression

transverse compression are more consistent with the experimental results.

7 Influence of loading velocity for spruce microstructure deformation

7.1 Loading velocity influence on wood deformation in axial compression condition

Numerical simulations of several loading velocities are performed to analyze loading rate influence on wood microstructure deformation. The model of RVE with hexagon pores in Fig. 8 is adopted to discuss loading velocity influence on wood response. Loading velocities of quasi-static, 5 m/s and 50 m/s are considered. For axial compression loading, stress–strain curve comparison of different compression velocities is shown in Fig. 20. It shows that the stress–strain curves are similar in the plastic plateau phase. The compaction strains are almost consistent for the three loading velocities. The tiny difference reflects that quasi-static loading is

with the lowest strain of the initial plateau stress. The loading velocity of 50 m/s is with the higher initial plateau stress.

Deformation processes of different loading velocities under axial compression are shown in Fig. 21. It indicates that wood microstructure deformation is affected by loading velocity. For quasi-static and 5 m/s loading, wood failure mode is mainly 45° shear sliding. When the loading velocity is 50 m/s, fold and collapse occur. There is no shear sliding in the deformation process. It shows that loading velocity affects greatly wood microstructure failure mode. High loading velocity brings wood structure abrupt damage. Low loading velocity is with relatively stable deformation of shear sliding, and the stress–strain curve is much smoother.

7.2 Loading velocity influence on wood deformation in transverse compression condition

Loading velocity influence on wood transverse compression is analyzed by numerical simulation. Being same as axial compression simulation, hexagon pore RVE is adopted and the loading velocities of quasi-static, 5 m/s and 50 m/s are taken in the numerical simulation. Stress–strain curves of different loading velocities are shown in Fig. 22. The stress–strain curves of quasi-static, 5 m/s and 50 m/s are almost similar in elastic and plastic deformation processes. The stress plateau and compaction strain are consistent for the three loading conditions. Comparing to axial compression in Fig. 20, transverse compression is with much lower plateau stress and smoother stress–strain curves. The compaction strain 0.66 of transverse compression is less than strain 0.85 of axial compaction.

The deformation processes of different loading velocities in transverse compression are shown Fig. 23. It indicates that the deformation is gradual and uniform for quasi-static, 5 m/s and 50 m/s loading. The cube models are compressed into flat, which is different from axial compression. There is no shear sliding phenomenon in the transverse compression. Comparing the axial with transverse compression, loading velocity in axial compression affects wood failure behavior greater than that of the transverse compression. The main failure mode is buckling in high velocity axial compression, it induces a unstable deformation. So the failure mode is easily affected by loading velocity in axial compression.

8 Conclusions

Representative volume elements (RVE) models of spruce microfibril and cell are proposed to analyze micromechanical properties and large deformation behavior using multi-scale finite element method. The equivalent mechanical properties of spruce cell material are given by the microfibril model
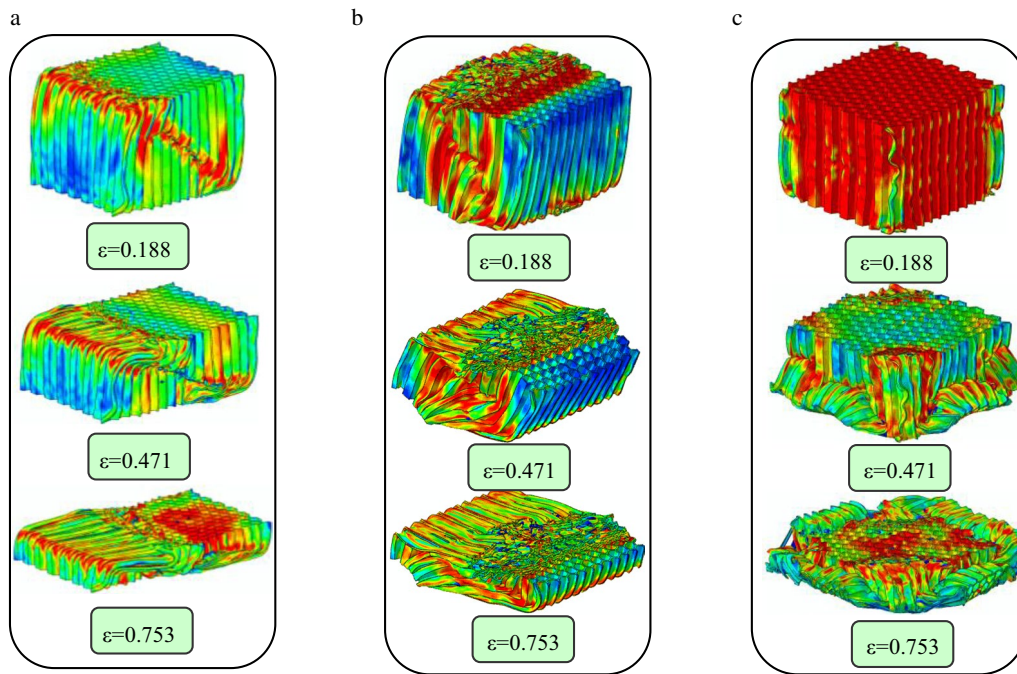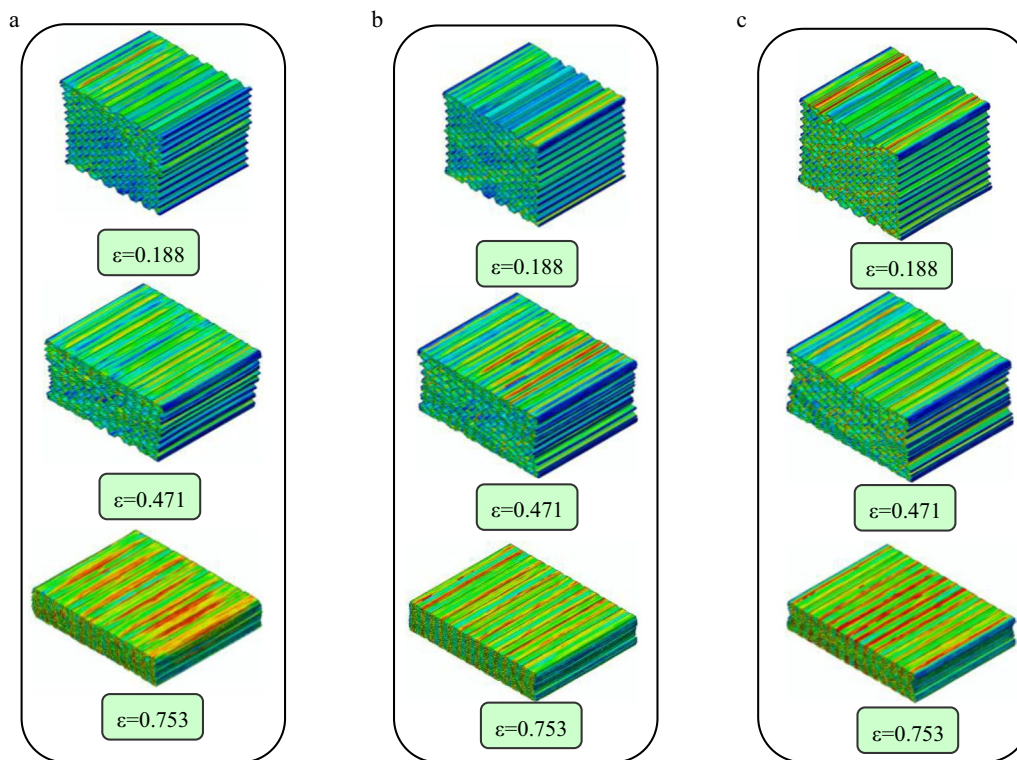
Fig. 21 Deformation comparison of different loading velocities under axial compression. **a** Quasi-static loading, **b** loading velocity is 5 m/s, **c** loading velocity is 50 m/s
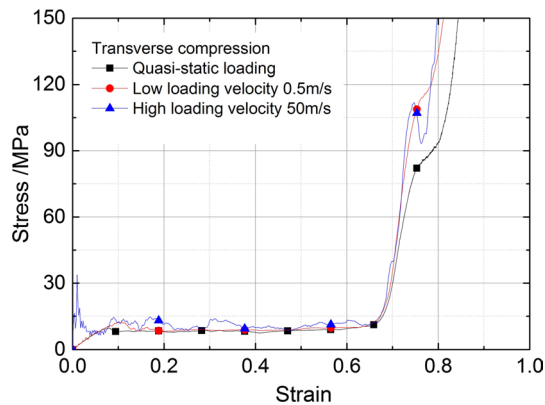
Fig. 22 Stress-strain curve comparison of different loading velocities under transverse compression

compression simulation. Two kinds of RVE models with hexagon and circular pores are adopted to simulate spruce microstructure large deformation under axial and transverse compression loading. The numerical simulation shows the simplified model with hexagon pores is better to reflect wood compression behavior. The RVE model deformation and the failure modes lead to the elastic, stress plateau and compaction deformation phases of wood stress–strain curve. The 45° shear sliding and buckling collapse are the main failure modes for wood axial compression. Transverse compression is with cell wall folding and collapse. Loading velocity influence on spruce microstructure deformation is given by several velocity compression simulations. It indicates loading velocity affect greatly wood microstructure failure modes.

Fig. 23 Deformation comparison of different loading velocities under transverse compression. **a** Quasi-static loading, **b** loading velocity is 5 m/s, **c** loading velocity is 50 m/s

References

1. Oudjene, M., Khelifa, M.: Elasto-plastic constitutive law for wood behaviour under compressive loadings. Constr. Build. Mater. **23**, 3359–3366 (2009)

2. Wang, D., Lin, L.Y., Fu, F.: Deformation mechanisms of wood cell walls under tensile loading: a comparative study of compression wood (CW) and normal wood (NW). Cellulose **27**, 4161–4172 (2020)

3. Bader, M., Nemeth, R., Konnerth, J.: Micromechanical properties of longitudinally compressed wood. Holz. Roh. Werkst. **77**, 341–351 (2019)

4. Kojima, E., Yamasaki, M., Imaeda, K., et al.: Effects of thermal modification on the mechanical properties of the wood cell wall of soft wood: behavior of S2 cellulose microfibrils under tensile loading. J. Mater. Sci. **55**, 5038–5047 (2020)

5. Amer, M., Kabouchi, B., Rahout, M., et al.: Mechanical properties of clonal eucalyptus wood. Int. J. Thermophys. **42**, 1–15 (2021)

6. Dou, Q.B., Wu, K.R., Suo, T., et al.: Experimental methods for determination of mechanical behaviors of materials at high temperatures via the split Hopkinson bars. Acta Mech. Sin. **36**, 1275–1293 (2020)

7. Song, B., Chen, W.: Dynamic stress equilibration in split Hopkinson pressure bar tests on soft materials. Exp. Mech. **44**, 300–312 (2004)

8. Lu, B.J., Li, J.R., Tai, H.C., et al.: A facile ionic-liquid pretreatment method for the examination of archaeological wood by scanning electron microscopy. Sci. Rep. UK **9**, 13253 (2019)

9. Song, J., Fan, C., Ma, H., et al.: Crack deflection occurs by constrained microcracking in nacre. Acta Mech. Sin. **34**, 143–150 (2018)

10. Oliver, M., Kim, C.K., Matthias, W., et al.: Performance of thermomechanical wood fibers in polypropylene composites. Wood. Mater. Sci. Eng. **15**, 114–122 (2020)

11. Adalian, C., Morlier, P.: A model for the behavior of wood under dynamic multiaxial compression. Compos. Sci. Technol. **61**, 403–408 (2001)

12. Reiterer, A., Lichtenegger, H., Fratzl, P., et al.: Deformation and energy absorption of wood cell walls with different nanostructure under tensile loading. J. Mater. Sci. **36**, 4681–4686 (2001)

13. Gong, M., Smith, I.: Effect of load type on failure mechanisms of spruce in compression parallel to grain. Wood Sci. Technol. **37**, 435–445 (2004)

14. Johnson, W.: Historical and present-day references concerning impact on wood. Int. J. Impact Eng. **4**, 161–174 (1986)

15. Reid, S.R., Peng, C.: Dynamic uniaxial crushing of wood. Int. J. Impact Eng. **19**, 531–570 (1997)

16. Speck, T.: The mechanics of Norway spruce [picea abies (L.) Karst]: mechanical properties of standing trees from different thinning regimes. For. Ecol. Manag. **135**, 45–62 (2000)

17. Widehammar, S.: Stress-strain relationships for spruce wood: influence of strain rate, moisture content and loading direction. Exp. Mech. **44**, 44–48 (2004)

18. Buchar, J., Rolc, S., Lisy, J. et al.: Model of the wood response to the high velocity of loading. In: 19th International Symposium of Ballistics. pp. 7–11 (2001)

19. Holmgren, S.E., Svensson, B.A., Gradin, P.A., et al.: An encapsulated split Hopkinson pressure bar for testing of wood at elevated strain rate, temperature, and pressure. Exp. Tech. **32**, 44–50 (2008)

20. Vural, M., Ravichandran, G.: Dynamic response and energy dissipation characteristics of balsa wood: experiment and analysis. Int. J. Solids Struct. **40**, 2147–2170 (2003)

21. Uhmeier, A., Salmen, L.: Influence of strain rate and temperature on the radial compression behavior of wet spruce. J. Eng. Mater. Technol. ASME **118**, 289–294 (1996)

22. Zhong, W.Z., Song, S.C., Huang, X.C., et al.: Research on static and dynamic mechanical properties of spruce wood by three loading directions. Chin. J. Theor. Appl. Mech. **43**, 1141–1150 (2011)

23. Zhong, W.Z., Song, S.C., Chen, G., et al.: Stress field of orthotropic cylinder subjected to axial compression. Appl. Math. Mech. **31**, 305–316 (2010)

24. Frantisek, S., Petr, K., Martin, B., et al.: Modelling of impact behaviour of European beech subjected to split Hopkinson pressure bar test. Compos. Struct. **245**, (2020)

25. Keckes, J., Burgert, I., Frühmann, K., et al.: Cell-wall recovery after irreversible deformation of wood. Nat. Mater. **2**, 810–813 (2003)

26. Clair, B., Thibaut, B.: Shrinkage of the gelatinous layer of poplar and beech tension wood. Iawa. J. **22**, 121–131 (2001)

27. Salmén, L.: Micromechanical understanding of the cell-wall structure. C. R. Biol. **327**, 873–880 (2004)

28. Li, Z., Zhan, T., Eder, M., et al.: Comparative studies on wood structure and microtensile properties between compression and opposite wood fibers of Chinese fir plantation. J. Wood. Sci. **67**, 1–6 (2021)

29. Jäger, A., Bader, T., Hofstetter, K., et al.: The relation between indentation modulus, microfibril angle, and elastic properties of wood cell walls. Compos. A **42**, 677–685 (2011)

30. Vasic, S., Smith, I., Landis, E.: Finite element techniques and models for wood fracture mechanics. Wood Sci. Technol. **39**, 3–17 (2005)

31. Vasic, S., Smith, I.: Bridging crack model for fracture of spruce. Eng. Fract. Mech. **69**, 745–760 (2002)

32. Dubois, F., Randriambololona, H., Petit, C.: Creep in wood under variable climate conditions: numerical modeling and experimental validation. Mech. Time-Depend. Mat. **9**, 173–202 (2005)

33. Flores, E.I.S., Friswell, M.I.: Multi-scale finite element model for a new material inspired by the mechanics and structure of wood cell-walls. J. Mech. Phys. Solids **60**, 1296–1309 (2012)

34. Flores, E.I.S., Neto, E.A.S., Pearce, C.: A large strain computational multi-scale model for the dissipative behavior of wood cell-wall. Comp. Mater. Sci. **50**, 1202–1211 (2011)

35. Clouston, P.L., Lam, F.: Computational modeling of strand-based wood composites. J. Eng. Mech. **127**, 844–851 (2001)

36. Li, P., Guo, Y.B., Shim, V.P.W.: Micro and mesoscale modelling of the response of transversely isotropic foam to impact: a structural cell-assembly approach. Int. J. Impact Eng. **135**, (2020)

37. Talebi, S., Sadighi, M., Aghdam, M.M.: Numerical and experimental analysis of the closed-cell aluminium foam under low velocity impact using computerized tomography technique. Acta Mech. Sin. **35**, 144–155 (2019)

38. Trtik, P., Dual, J., Keunecke, D., et al.: 3D imaging of microstructure of spruce wood. J. Struct. Biol. **159**, 46–55 (2007)

39. Smith, I., Landis, E., Gong, M.: Fracture and Fatigue in Wood. Wiley, Chichester (2003)

40. Xu, P., Donaldson, L.A., Gergely, Z.R., et al.: Dual-axis electron tomography: a new approach for investigating the spatial organization of wood cellulose microfibrils. Wood Sci. Technol. **41**, 101–116 (2007)

41. Donaldson, L.A., Singh, A.P.: Bridge-like structures between cellulose microfibrils in radiata pine (Pinus radiata D. Don) kraft pulp and holocellulose. Holzforsch. Int. J. Biol. Chem. Phys. Tech. Wood. **52**, 449–454 (1998)

42. Andersson, S., Wikberg, H., Pesonen, E., et al.: Studies of crystallinity of Scots pine and Norway spruce cellulose. Trees **18**, 346–353 (2004)

43. Andersson, S., Serimaa, R., Paakkari, T., et al.: Crystallinity of wood and the size of cellulose crystallites in Norway spruce (Picea abies). J. Wood. Sci. **49**, 531–537 (2003)

44. Chen, W., Lickfield, G.C., Yang, C.Q.: Molecular modeling of cellulose in amorphous state. Part I: model building and plastic deformation study. Polymer. **45**, 1063–1071 (2004)

45. Hofstetter, K., Hellmich, C., Eberhardsteiner, J.: Development and experimental validation of a continuum micromechanics model for the elasticity of wood. Eur. J. Mech. A. **24**, 1030–1053 (2005)

46. Kilingar, N.G., Kamel, K.E.M., Sonon, B., et al.: Computational generation of open-foam representative volume elements with morphological control using distance fields. Eur. J. Mech. A **78**, (2019)